PERGAMON

International Journal of Solids and Structures 39 (2002) 6103–6120

INTERNATIONAL JOURNAL OF SOLIDS and STRUCTURES

www.elsevier.com/locate/ijsolstr

Transient elastic wave propagation in a spherically symmetric bimaterial medium modeling the thorax

Quentin Grimal, Salah Naili *, Alexandre Watzky

Laboratoire de Mécanique Physique, CNRS UMR 7052 B2OA Faculté des Sciences et Technologie, Université Paris XII-Val de Marne 61, Avenue du Général de Gaulle, 94010 Créteil Cédex, France

Received 1 April 2002; received in revised form 18 July 2002

Abstract

The transient response resulting from an impact wave on an elastic bimaterial, made out of a "hard" medium and a "soft" medium, welded at a spherical interface, have been investigated by using an integral transform technique. This technique permits isolation of the pressure and shear waves contributions to the wave field. The method of solution makes use of the generalized ray/Cagniard-de Hoop (GR/CdH) method associated with a "flattening approximation" (FA) technique, similar to the Earth flattening transformation used in geophysics. The GR/CdH method and the FA technique are briefly presented, together with their numerical implementations. The FA has proved to be useful in geophysical application, however, as far as the authors know, it has never been investigated for other applications. For the purpose of this paper, numerous tests of the method have been performed in order to check that the FA is appropriate to compute transient responses in the special case presented here. We could determine appropriate values for some parameters involved in the FA. This paper follows Grimal et al. [Int. J. Solid Struct. 39 (2002) 5345] in which we investigated the same bimaterial with a plane—instead of spherical—interface. Numerical examples are concerned with the propagation of an impact wave in the thorax modeled as a bimaterial (thoracic wall-lung). In addition to the effects of the weak coupling of the two media already observed in our previous study, we found that, for interface curvatures characteristic of those measured in the thorax, focalization of energy is manifest.

Keywords: Transient; Wave; Stratified media; Cagniard-de Hoop; Impact; Thorax; Earth flattening

1. Introduction

The study of transient elastic waves in layered media is of interest for many applications. In the past ten decades, geophysicians have developed powerful analytical and numerical methods to solve problems derived from seismology; these methods have then been exported to other fields of mechanical engineering such as non-destructive evaluation of composites. Seismology is concerned with wave propagation in Earth. Layered models with spherical symmetry (concentric layers) are a good representation of the Earth

* Corresponding author. Tel.: +33-1-4517-1445; fax: +33-1-4517-1433.
E-mail addresses: grimal@univ-paris12.fr (Q. Grimal), naili@univ-paris12.fr (S. Naili), watzky@univ-paris12.fr (A. Watzky).

0020-7683/02/$ - see front matter
PII: S0020-7683(02)00469-9

geometry but they lead to complicated equations as compared to those ruling planarly layered media. Seismologists have been looking for transformations—Earth flattening approximations (FA)—, acting not only upon the coordinate system but also on the media properties, to allow for the study of wave propagation in a model of spherical Earth by using existing analytical and numerical methods for "flat" Earth models. Thinking in terms of geometrical rays, the idea is to study curved rays in a flat structure instead of straight rays in a spherical structure. This is achieved through the introduction in the flat representation of depth-dependence media parameters, so that the rays are continuously refracted.

The main reasons and advantages for using the FA are (i) most of the formalisms and analytical methods dedicated to layered media (scattering matrix formalism, exact generalized ray (GR) theory,...), cannot be used in spherical geometry (i.e., with a spherical system of coordinates); (ii) FA avoid some algebraic and numerical difficulties appearing when manoeuvring with Bessel functions that occur in the spherical formulation (Arora et al., 1996); (iii) minimal changes are required to introduce the FA in the numerical programs dedicated to planarly layered media.

Unlike conformal transformations used for the resolution of the Laplace's equation with complex boundary shapes, FA are not exact—except for the study of Love waves (Biswas and Knopoff, 1970). As a matter of consequence, several FA have been investigated for different wave propagation studies. However, most of the authors (see Aki and Richard, 1980, p. 463; Müller, 1971; Chapman, 1973; Arora et al., 1996) have used the same set of transformations—derived from the kinematic properties of geometrical rays—for the coordinates and the wave velocities. On the other hand, many transformations have been proposed for the mechanical parameters (Young's modulus and Poisson's ratio or, alternatively, Lamé's coefficients), for different wave problems (study of body or surface waves, *SH* or *P–SV* problems,...).

The present paper follows a study (Grimal et al., 2002b) in which the wave propagation in a bimaterial medium, with a plane interface, modeling the thorax was investigated; the bimaterial represented the thoracic wall (medium 1) and the lung (medium 2); a point source generated a wave motion in medium 1 and the response was computed in medium 2.

Our work is part of a preliminary study aiming at characterizing the strains and stresses undergone by thoracic tissues during a non-penetrating impact. This is of interest to the defense industry concerned with high velocity impacts (design of bulletproof jackets) and to the automotive industry concerned with lower velocity impacts (crash safety systems). The necessity for investigations on the interaction of stress waves with thoracic tissues has been underlined by Fung et al. (1988) and Yen et al. (1988). Indeed, the impact wave is supposed to play an important role in the occurrence of lung injuries.

In our previous works (Grimal et al., 2002a; Grimal et al., 2002b), the interface between the two media was plane; we could show that, due to the weak acoustic coupling between the two media, the energy was propagated in a relatively narrow zone in medium 2 (a few centimeters around an axis passing through the source and perpendicular to the interface); this has been recognized as a focalization effect. In the present study, the wave propagation in the same bimaterial model, but with a spherical interface, is investigated (Fig. 1); our purpose is to quantify the additional focalization due to the curvature of the interface.

In this paper, we use the flattening technique together with the exact three-dimensional generalized ray/Cagniard-de Hoop (GR/CdH) method. The GR/CdH method is a very powerful tool for the study of transient wave propagation in planarly layered media. It allows to compute exact solutions directly in the time domain; relevant references for these methods are Aki and Richard (1980), Kennett (1983) and Pao and Gajewski (1977). The GR method splits the solution for the wave motion at some point of the media (called the receiver) in a sum of contributions. Each contribution is associated with a "GR path", i.e., with a succession of transmissions and reflections (with or without mode conversion) at each interface between the source and the receiver. Finally, a GR is defined both by a path and by a sequence of modes of propagation (longitudinal or transverse polarization), i.e., one mode per layer crossed. Formally, each GR is an integral transform representation of a contribution to the solution; they are obtained in a Fourier–Laplace domain dual of the space–time domain. The Cagniard-de Hoop method applies to each GR

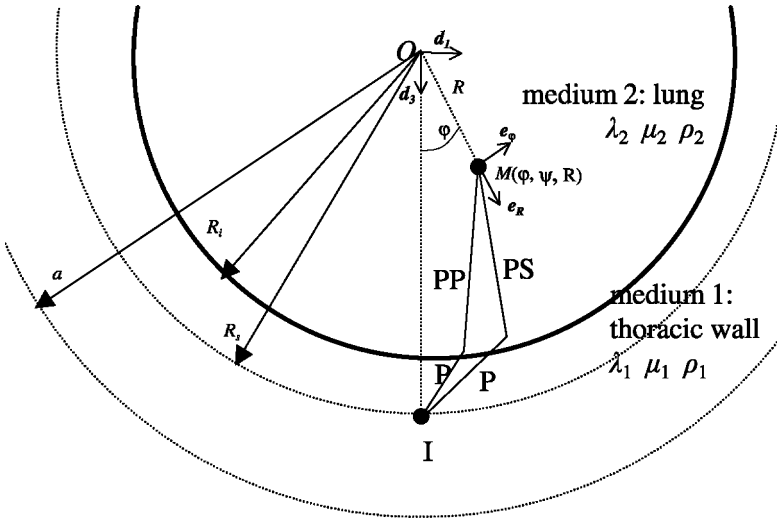

Fig. 1. Configuration and coordinate sytems in the spherical representation.

integral; in essence, it is a mathematical trick to avoid integrations over the frequency, or over the wave number, required to transform the solutions back to the space–time domain. Gilbert and Helmberger (1972) have shown that the GR/CdH method can be used in an approximate way in spherical geometry. However, in our study, we choose to apply the *exact* GR/CdH method to a flat representation, equivalent to a spherically symmetric model, obtained with an *approximate* flattening transformation.

In a previous paper (Grimal et al., 2002b), the GR/CdH method and its numerical implementation in a bimaterial medium with a plane interface have been described. The aim of this paper is to present the flattening transformation procedure, associated with the exact three-dimensional GR/CdH method. We discuss the choice of some parameters involved in the transformation for the length and time scales related to our biomechanical application. We not only give the transformations for the coordinates and mechanical properties as used in geophysics, but also we propose some procedures to validate the method before it can be used with length and times scales different to those used in geophysical applications. As far as we know, the FA have only been used for geophysical applications; however, they are of interest to other fields of mechanical engineering concerned with transient wave propagation in elastic media.

With this introduction as background, we present in Section 2 the basic set of transformations used to derive the plane representation (Fig. 2) equivalent to the spherical representation illustrated in Fig. 1. For the sake of completeness, the main steps of the GR/CdH method for plane-layered media are given. Then we expose the method used to validate the transformation and to choose the parameters. Finally, Section 3 is devoted to the biomechanical application.

2. Model and method of solution

2.1. Configuration and definitions

The model geometry is illustrated in Fig. 1; it consists of two media with concentric spherical boundaries, the center of the spheres is the point O. With this model geometry, we will use both spherical and Cartesian coordinates systems, together with their associated basis. The spherical coordinates are denoted by (φ, ψ, R)

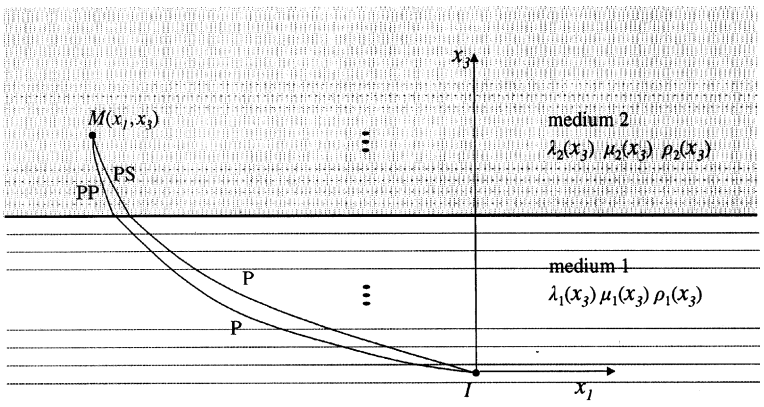

Fig. 2. Configuration and coordinate sytem in the equivalent plane representation.

Table 1
Lamé's coefficients, densities and wave speeds for media 1 and 2

	$\lambda \times 10^6$ (Pa)	$\mu \times 10^6$ (Pa)	ρ (kg m^{-3})	c_S (m s^{-1})	c_P (m s^{-1})
Medium 1	1126	562	1000	750	1500
Medium 2	0.034	0.008	500	4	10

c_S and c_P are the pressure and shear waves speeds.

and the associated orthonormal spherical basis is denoted by $(\mathbf{e}_\varphi, \mathbf{e}_\psi, \mathbf{e}_R)$. The Cartesian coordinates originating at point O are denoted by (d_1, d_2, d_3) and the associated orthonormal basis is denoted by $(\mathbf{d}_1, \mathbf{d}_2, \mathbf{d}_3)$. Let I be a point on axis $\mathbf{d}_3$. The spherical coordinates are defined with respect to the Cartesian basis as follows. For a given point M, R is taken to be the distance OM; φ is taken to be the angle between $\mathbf{d}_3$ and $\mathbf{e}_R$; finally, ψ is the angle between the projection of **OM** in the plane defined by $(\mathbf{d}_1, \mathbf{d}_2)$ and $\mathbf{d}_1$. Due to symmetry, the problem is ψ-independent; consequently, in the Cartesian coordinate system, we will only use the distances $d = \sqrt{d_1^2 + d_2^2}$ and d_3.

The media are assumed homogeneous, isotropic and linearly elastic; we will use the Lamé's elastic parameters λ and μ, and the mass density ρ (see Table 1). At the—spherical—interface, the media are welded. Pressure and shear wave speeds are respectively defined by $c_P = \sqrt{(\lambda + 2\mu)/\rho}$ and $c_S = \sqrt{\mu/\rho}$. Wave slownesses are defined as $s_{P,S} = 1/c_{P,S}$ where P or S must be used for pressure and shear waves respectively. All through the paper, each time a comma appears between P and S means that the quantities relative to P-waves or SV-waves respectively must be used. The particle velocity and the Cauchy stress tensor are respectively denoted by $\mathbf{v}$ and σ. The elastodynamics problem will be solved for the six components of the motion-stress vector whose expression in the spherical system of coordinates is: $\mathbf{b} = (v_\varphi, v_\psi, v_R, -\sigma_{R\varphi}, -\sigma_{R\psi}, -\sigma_{RR})^{\mathrm{T}}$ (here 'T' means transpose). The welded-interface condition requires the continuity of $\mathbf{b}$ at the interface.

The wave motion is generated by a point source, located in medium 1 at point I (Fig. 1) of coordinate $(0, 0, d_{3;I})$ in the Cartesian frame, or alternatively, of coordinate $(0, 0, R_I)$ in spherical frame. Computations have been made for two types of sources (see Grimal et al., 2002b): a buried point force with direction $\mathbf{d}_3$ (in this case, medium 1 is unbounded), and a point force with direction $\mathbf{d}_3$ at a free spherical surface defined by $R = R_I$ (in this case, medium 1 is bounded). For later use, we define $z = R_I - d_3$, so that the source is placed at $z = 0$. Now, by using the FA (see Section 2.2), we are going to achieve a model configuration similar to that investigated in Grimal et al. (2002b).

2.2. The flattening transformations (FA)

In order to compute the transient response resulting from an impact wave on a layered medium, we use a set of transformations—similar to the earth flattening approximation used in geophysics—that defines a "flat" representation equivalent to the "spherical" representation described above; in the "flat" representation, the spherical interface is replaced by a plane interface (Fig. 2). In what follows, subscripts s and f will respectively refer to the spherical representation and its equivalent flat representation. Another Cartesian reference frame is associated with the flat representation (Fig. 2): the coordinates originating at point I (as defined in the spherical configuration above) are denoted by (x_1, x_2, x_3), and the associated orthonormal basis by $(\mathbf{x}_1, \mathbf{x}_2, \mathbf{x}_3)$, where $\mathbf{x}_3$ (corresponding to $-\mathbf{d}_3$) is perpendicular to the—plane—interface. (Note that the vectors of this basis have the same directions as the vectors of the Cartesian basis $(\mathbf{d}_1, \mathbf{d}_2, \mathbf{d}_3)$ defined in the model with the spherical geometry.) In the flat representation, media 1 and 2 are unbounded in directions $\mathbf{x}_1$ and $\mathbf{x}_2$. Making use of the axisymmetry of the problem, we will, without loss in generality, make all the computations for points in the $(\mathbf{x}_1, \mathbf{x}_3)$ plane.

The flattening transformations leading to the "flat" representation involve both geometrical transformations (acting on the coordinate system) and transformations of the mechanical parameters. The set of FA may be split into two groups. First, transformations for the coordinates and the wave speeds are defined by the kinematic properties of the geometrical ray (far field) theory (Chapman, 1973; Müller, 1971), i.e., these FA introduce an approximation that is optimum for a description of wave propagation with the aid of geometrical rays—we will assume, following Müller (1971), that the approximation is also valid for calculations with the exact theory. Coordinates and wave speeds in the equivalent flat representation are given by

$$x_1 = a\varphi, \quad x_3 = a \ln\left(\frac{R}{a}\right), \quad c_{P;f}(x_3) = \frac{a}{R} c_{P;s}, \quad c_{S;f}(x_3) = \frac{a}{R} c_{S;s}, \tag{1}$$

where a is a reference radius to be discussed below, and "ln" denotes the Neperian logarithm. Second, the computation of stresses—and not only displacements and travel times, as for most geophysical applications—requires some additional transformations given by Chapman (1973). The mechanical parameters in the flat representation are given by

$$\lambda_f(x_3) = (R/a)^m \lambda_s, \quad \mu_f(x_3) = (R/a)^m \mu_s, \quad \rho_f(x_3) = (R/a)^{m+2} \rho_s. \tag{2}$$

Once solutions have been computed in the flat representation, the motion-stress vector $\mathbf{b}$ corresponding to the spherically symmetric problem is calculated by using the following transformations

$$\mathbf{v}_f \mapsto \mathbf{v}_s = (a/R)^l \mathbf{v}_f, \qquad \sigma_f \mapsto \sigma_s = (a/R)^{l+m+1} \sigma_f, \tag{3}$$

where vectors and tensors with subscripts f and s are expressed in the Cartesian basis $(\mathbf{x}_1, \mathbf{x}_2, \mathbf{x}_3)$ and in the spherical basis $(\mathbf{e}_\varphi, \mathbf{e}_\psi, \mathbf{e}_R)$ respectively. Thus, for instance, the first transformation given by Eq. (3) allows to obtain the components of the vector $\mathbf{v}_s$ in the basis $(\mathbf{e}_\varphi, \mathbf{e}_\psi, \mathbf{e}_R)$ from the components of the vector $\mathbf{v}_f$ calculated in the basis $(\mathbf{x}_1, \mathbf{x}_2, \mathbf{x}_3)$. The parameters m and l will be discussed in the next section. We could not find any study that establishes the degree of validity of these last five transformations (Chapman (1973) pointed out the difficulty of doing this), however, similar forms of the transformations have yielded exact solutions in some specific cases (Biswas and Knopoff, 1970) and many authors have used them with success (see, e.g., Biswas, 1972; Arora et al., 1996; Bhattacharya, 1996).

In this study, transient responses in the equivalent flat representation, illustrated in Fig. 2, are calculated with the exact three-dimensional GR/CdH method. In the following subsections, we write down the main steps of the method; more details on the GR/CdH method are given in Grimal et al. (2002b) and a thorough presentation can be found in Van der Hijden (1987). In what follows, we will omit the subscript f since all

the equations will be written for the flat representation. Before we can use the GR/CdH method, media 1 and 2 of the flat representation (which density and Lamé coefficients, given by Eq. (2), are continuous functions of x_3) must be sliced into thin homogeneous layers, so that λ, μ and ρ are constant in each thin layer. This last approximation—substituting to a media with continuously varying properties, a stack of layers with constant properties—has been extensively studied by geophysicians (see Aki and Richard, 1980 p. 385) and it has been shown that doing a sufficiently fine discretization yields accurate results; the influence of the spatial discretization will be discussed in the following section.

2.3. Governing equations, boundary and initial conditions in the flat configuration

In each homogeneous layer illustrated in Fig. 2, the equation of motion is

$$\partial_j \sigma_{ij} - \rho \partial_t v_i = -f_i, \tag{4}$$

where ∂_j and ∂_t denote partial derivatives with respect to x_j and to time respectively. Einstein's summation convention is used. The term f_i stands for a volume density of force. The time derivative of Hooke's constitutive law for an elastic isotropic medium can take the form

$$\partial_t \sigma_{ij} - \lambda \delta_{ij} \delta_{pq} \partial_p v_q - \mu(\partial_i v_j + \partial_j v_i) = 0, \tag{5}$$

where δ_{ij} is the Kronecker symbol.

The initial condition is that all the layers are at rest for $t < 0$. For the purposes of the present study, we have made calculations with two types of sources: (i) for a buried point force we take $\mathbf{f} = (0, 0, f_0 \phi(t) \delta(x_1, x_2, x_3))$, where $\delta(x_1, x_2, x_3)$ is the three-dimensional Dirac function, f_0 is the amplitude of the source and $\phi(t)$ defines the temporal shape of the source; (ii) for a point force at the free surface, we take $\mathbf{f} = (0, 0, 0)$ in (4) and, in addition to (4) and (5), the boundary conditions at the free surface (defined by $x_3 = 0$) require

$$\begin{aligned} &\sigma_{33}(x_1, x_2, 0, t) = f_0 \phi(t) \delta(x_1, x_2), \\ &\sigma_{13}(x_1, x_2, 0, t) = \sigma_{23}(x_1, x_2, 0, t) = 0, \end{aligned} \tag{6}$$

where $\delta(x_1, x_2)$ is the two-dimensional Dirac function. In addition, the welded contact condition at the interfaces requires that the motion-stress vector is continuous at the interfaces between two adjacent media.

2.4. The method of solution in the flat representation

First, the solution of the elastodynamics problem for the model configuration illustrated in Fig. 2 is found in a Laplace–Fourier transform-domain after some algebraic manipulations; then the Cagniard-de Hoop method is used to obtain the solution in the space-time domain. In what follows, we recall the solution for an infinite, or semi-infinite medium, as presented in Grimal et al. (2002b). Then, we present the formalism for the derivation of the solution in a layered medium.

2.4.1. Solution in a homogeneous medium

The first step of the method consists in writing Eqs. (4)–(6) in a transformed domain in which first order ordinary differential equations are solved. For this purpose, the one-sided Laplace transform with respect to time and the Fourier transform with respect to the x_1- and x_2-coordinates are used. The Laplace and Fourier transform parameters are respectively p and $pk_l (l = 1, 2)$. Quantities in the transformed domain are indicated with $\tilde{.}$ and Laplace-transformed quantities by $\hat{.}$.

The solution in the transformed domain is obtained as a sum of six wave amplitudes. Formally, the solution for any component of the motion-stress vector $\tilde{\mathbf{b}} = (\tilde{v}_1, \tilde{v}_2, \tilde{v}_3, -\tilde{\sigma}_{13}, -\tilde{\sigma}_{23}, -\tilde{\sigma}_{33})^{\mathrm{T}}$ takes the form

$$\tilde{b}_i = \hat{\phi}(p) \times \sum_{n=1}^{6} \left\{ D_{in} W_n \exp[\pm p s_3^{P,S} x_3] \right\} = \sum_{n=1}^{6} \tilde{b}_i^n. \tag{7}$$

In the formalism used, the terms D_{in} are stocked in a matrix whose lines and columns are associated with components $\tilde{b}_i$ and with the polarization of a wave respectively; and W_n is a source term standing for the amplitude of a wave of a given polarization emitted by the source. For the purposes of the present paper, we have used source terms corresponding to three types of sources: buried source of strain rate (explosion) (Van der Hijden, 1987), buried point force (Van der Hijden, 1987), and point force acting at a free surface (Grimal et al., 2002b). The exponential term is a phase term accounting for the propagation of a wave. The term $s_3^{P,S} = (s_{P,S}^2 + k_1^2 + k_2^2)^{1/2}$ is the slowness along the x_3-axis for P- or S-waves. Each term b_i^n of the sum in Eq. (7) is called a *generalized ray* (GR).

The solution in the Laplace domain for one of the six GR is obtained by applying the inverse Fourier transform

$$\hat{b}_j^n(\mathbf{x}, p) = \hat{\phi}(p) \times (p/2\pi)^2 \int_{-\infty}^{\infty} \int_{-\infty}^{\infty} D_{jn}(k_1, k_2) W_n(k_1, k_2) \exp\left[-p(\mathrm{i}k_1 x_1 + \mathrm{i}k_2 x_2 \mp s_3^{P,S} x_3) \right] \mathrm{d}k_1 \, \mathrm{d}k_2. \tag{8}$$

The Laplace domain solution for a component of the motion-stress vector in an infinite medium or in a semi-infinite medium (with the source acting at the free surface), for a point force source of direction $\mathbf{x}_3$, takes the form

$$\hat{b}_j(\mathbf{x}, p) = \hat{b}_j^4(\mathbf{x}, p) + \hat{b}_j^5(\mathbf{x}, p), \tag{9}$$

where $\hat{b}_j^4(\mathbf{x}, p)$ and $\hat{b}_j^5(\mathbf{x}, p)$ are the P- and SV-wave contributions to the solution respectively (SH-wave contribution is zero because the loading is along the x_3-axis). (The numbering, in relation with the polarizations, is consistent with the formalisms used in Van der Hijden (1987) and Grimal et al. (2002b).)

2.4.2. Solution for the layered medium

Let us write the solution for waves emitted in medium 1 and transmitted in medium 2; this solution has been used to obtain the numerical results presented in Section 3. In Grimal et al. (2002b), we have been concerned with a bimaterial, hence few GR were involved (we computed up to four); in the present paper, the flat representation consists in a layered medium with numerous interfaces. The computation of the exact solution requires, in theory, to compute all the GR; however, since we are interested in the transmission of energy from medium 1 to medium 2, a substantial simplification can be made. Among the many interfaces, only the one that separates the two media and corresponds to a *physical* interface, at which there is a significative jump (discontinuity) in the mechanical properties. Except for this interface, almost all the energy is transmitted between two sub-layers, i.e., there is neither reflection nor conversion of the wave (the effect of the additional interfaces within media 1 and 2, introduced by the FA, is basically to deviate the energy, that is, to "bend the rays"). Thus, very much like in Grimal et al. (2002b), we will compute only four GR; the solution for a motion-stress vector component in the Laplace-domain is, for both types of sources (see Eq. (9))

$$\hat{b}_j(\mathbf{x}, p) = \hat{b}_j^{P \to P}(\mathbf{x}, p) + \hat{b}_j^{P \to S}(\mathbf{x}, p) + \hat{b}_j^{S \to P}(\mathbf{x}, p) + \hat{b}_j^{S \to S}(\mathbf{x}, p), \tag{10}$$

where the meaning of the notations is as follows. Let the Greek letters α and β stand for P or S symbols in media 1 and 2 respectively, then the notation $\alpha \to \beta$ is read: the GR corresponding to the wave of polarization α emitted in medium 1, propagated—with no loss of energy—in each sub-layer of medium 1, and transmitted in medium 2 as a wave of polarization β up to the receiver (in medium 2, this wave is also transmitted with no loss of energy at each sub-interface). In the case of a force at the free surface, we do not include in the computation of the solution the waves reflected at the free surface and transmitted in medium

2; hence the solution computed will be valid up to the arrival time of the first wave that has undergone a reflection at the free surface.

Each of the terms in (10) is deduced from the solution (8) in the single-medium configuration. Many authors have shown with different formalisms (Aki and Richard, 1980; Kennett, 1983; Van der Hijden, 1987) that the interaction of waves with interfaces can be accounted for by introducing specific terms called "generalized transmission and reflection coefficients". Aside from the introduction of a transmission coefficient, the phase term $s_3^{P,S}x_3$ appearing in Eq. (8) is changed to account for the travel times in each homogeneous layer. Let n_1 and n_2 be the number of sub-layers introduced by the FA in media 1 and 2 respectively, with $n = n_1 + n_2$. The solution for each GR in the Laplace-domain, corresponding to a wave emitted in layer 1 and a receiver in layer n, takes the form

$$\hat{b}_j^{\alpha\to\beta}(\mathbf{x},p) = \hat{\phi}(p) \times \left(\frac{p}{2\pi}\right)^2 \int_{-\infty}^{\infty}\int_{-\infty}^{\infty} B_j^{\alpha\to\beta}(k_1,k_2) T_{\alpha\to\beta} \exp\left[-p\left(\mathrm{i}k_1 x_1 + \mathrm{i}k_2 x_2 + \sum_{y=1}^{n_1} s_3^{\alpha;y} h_y + \sum_{y=n_1+1}^{n} s_3^{\beta;y} h_y \right)\right] \mathrm{d}k_1 \mathrm{d}k_2, \tag{11}$$

where $s_3^{P,S;y} = (s_{P,S;y}^2 + k_1^2 + k_2^2)^{1/2}$; h_y is the thickness of a sub-layer and $T_{\alpha\to\beta}$ is the transmission coefficient at the "physical interface" between media 1 and 2 (all the other transmission coefficients are set equal to one; there is neither reflection nor conversion at these sub-interfaces). The term $B_j^{\alpha\to\beta}(k_1,k_2)$ accounts both for the coupling of the source to the medium, the component of **b**, and the type GR; it may also be written as

$$B_i^{\alpha\to\beta}(k_1,k_2) = D_{im}^{(n)} W_l^{(1)}, \tag{12}$$

where superscripts (n) and (1) stand for the layer number in which the quantities are evaluated. Subscripts l and m are associated with polarizations α and β respectively; like in Grimal et al. (2002b), l and m take the values 4 or 5 depending on the GR under study; for example, the ray denoted by $P \to S$ is associated with $l = 4$ and $m = 5$.

In the remainder of this subsection, we will describe the method used to transform each GR contribution (11) in the Laplace-transform domain back to the space–time domain, by applying the Cagniard-de Hoop (CdH) method.

Upon introducing the change of variables

$$\mathrm{i}k_1 = s\cos\theta - \mathrm{i}q\sin\theta, \qquad \mathrm{i}k_2 = s\sin\theta + \mathrm{i}q\cos\theta, \tag{13}$$

where θ and $r(0 \leqslant \theta < 2\pi, 0 \leqslant r < \infty)$ are the polar coordinates in the (x_1,x_2) plane; q is a real number and s is complex. Noting that $\mathrm{i}k_1x_1 + \mathrm{i}k_2x_2 = sr$, Eq. (11) becomes

$$\hat{b}_j^{\alpha\to\beta}(\mathbf{x},p) = \hat{\phi}(p) \times (p^2/4\mathrm{i}\pi^2) \int_{-\infty}^{\infty} \mathrm{d}q \int_{-\mathrm{i}\infty}^{\mathrm{i}\infty} B_j^{\alpha\to\beta}(s,q) T_{\alpha\to\beta} \exp\left[-p\left(sr + \sum_{y=1}^{n_1} s_3^{\alpha;y} h_y + \sum_{y=n_1+1}^{n} s_3^{\beta;y} h_y \right)\right] \mathrm{d}s. \tag{14}$$

In Eq. (14), the integration over the variable s lies along the imaginary axis. The CdH method consists in a deformation of the contour of integration away from this axis; this requires to extend the definition of the integrand in the complex s plane by analytic continuation. This cannot be achieved without a detailed analysis of the analyticity of the integrand (for a detailed discussion see Van der Hijden, 1987): if during its deformation, the contour crosses a singularity, another integral must be evaluated. Whether or not this happens depends on the location of the receiver with respect to the source and on the material properties; in the numerical examples presented in this paper the contour does not cross any singularity during its deformation (see Grimal et al., 2002b).

The next step of the method is to take τ to be the real variable—with the dimension of time—defined by

$$\tau = sr + \sum_{y=1}^{n_1} s_3^{\alpha;y} h_y + \sum_{y=n_1+1}^{n} s_3^{\beta;y} h_y. \tag{15}$$

The solution of this equation for $s(q,\tau)$ is the CdH contour for the GR under consideration. Considering the symmetry properties of both $B_j^{\alpha\to\beta}(s,q)$ and the contour, Eq. (14) can be rewritten as an integral over τ

$$\hat{b}_i^{\alpha\to\beta}(\mathbf{x},p) = \hat{\phi}(p) \times (p^2/2\pi^2) \int_{-\infty}^{\infty} \mathrm{d}q \int_{T(q)}^{\infty} \Im\left[B_i^{\alpha\to\beta}(s,q) T_{\alpha\to\beta}(s,q) \partial_\tau s\right] \exp[-p\tau]\,\mathrm{d}\tau, \tag{16}$$

where $\Im$ denotes the imaginary part and $T(q)$ is the minimum of τ on the contour; it corresponds to the point at which the contour intersects the real axis and is given by (Van der Hijden, 1987)

$$T(q) = \sum_{y=1}^{n_1} \frac{(s_{\alpha;y}^2 + q^2)^{1/2} h_y}{\cos\Theta_y(q)} + \sum_{y=n_1+1}^{n} \frac{(s_{\beta;y}^2 + q^2)^{1/2} h_y}{\cos\Theta_y(q)}, \tag{17}$$

the angles $\Theta_y(q)$ being defined through the equations

$$(s_{P,S;y}^2 + q^2)^{1/2} \sin\Theta_y(q) = s^0(q) \tag{18}$$

and

$$r = \sum_{y=1}^{n_1} h_y \tan\Theta_y(q) + \sum_{y=n_1+1}^{n} h_y \tan\Theta_y(q), \tag{19}$$

where $s^0(q)$ is given by the intersection of the Cagniard-de Hoop contour with the real axis.

Next, we must interchange the order of integration in Eq. (16), i.e., the integration over q must be performed first. The new limits of integration are $-Q(\tau)$ and $Q(\tau)$; they are solutions for q of the equation $\tau = T(q)$. Eq. (16) becomes

$$\hat{b}_i^{\alpha\to\beta}(\mathbf{x},p) = \hat{\phi}(p) \times (p^2/2\pi^2) \int_{T_\mathrm{a}}^{\infty} \left\{ \int_{-Q(\tau)}^{Q(\tau)} \Im\left[B_i^{\alpha\to\beta}(s,q) T_{\alpha\to\beta}(s,q) \partial_\tau s\right] \mathrm{d}q \right\} \exp[-p\tau]\,\mathrm{d}\tau, \tag{20}$$

where $T_\mathrm{a} = T(q=0)$ appears to be the arrival time of the wave associated with the GR denoted by $\alpha\to\beta$. In Eq. (20), the integration over τ has the form of a forward Laplace transform, the transformation back to the time domain can thus be done by inspection. Eventually, the space–time domain solution for the contribution of one GR is given by

$$\begin{cases} b_j^{\alpha\to\beta}(\mathbf{x},t) = 0 & \text{for} \quad 0 \leqslant t \leqslant T_\mathrm{a}, \\ b_j^{\alpha\to\beta}(\mathbf{x},t) = (1/2\pi^2)\partial_u\phi(t) \;*\; \int_{-Q(t)}^{Q(t)} \Im\left[B_j^{\alpha\to\beta}(s,q) T_{\alpha\to\beta}(s,q) \partial_t s\right] \mathrm{d}q & \text{for} \quad T_\mathrm{a} < t, \end{cases} \tag{21}$$

where $*$ denotes a convolution product.

Numerical computations. For each component $b_j(\mathbf{x},t)$ of the motion-stress vector, one must evaluate the Green's function, that is: (i) the integral appearing in (21) and its limits; and (ii) the Cagniard-de Hoop contour $s(\tau,q)$, given by (15), for each value of q under the integral. It is to note that for receivers on the x_3-axis (corresponding to axis $\mathbf{d}_3$), the integration over q can be evaluated analytically (see Grimal et al. (2002b)). In this former study, a method and its numerical implementation have been developed to compute expressions like (21) with $n_1 = n_2 = 1$; for the purposes of the present study, the program has been modified: the flattening transformations (1)–(3) have been implemented together with a procedure to generate the sub-layers accounting for the continuous variation of the mechanical parameters.

An inner product of the components of the motion-stress vector $\mathbf{b}$ yields the projection of the Poynting vector in direction $\mathbf{e}_R$: $P_R = v_\varphi \sigma_{\varphi R} + v_\phi \sigma_{\phi R} + v_R \sigma_{RR}$. Since we will only consider receivers close to axis $\mathbf{d}_3$ for which the angle φ is small, P_R is a very good approximation of the projection of the Poynting vector on $\mathbf{d}_3$, which we denote by P_3 (for the receiver locations used in this paper, the error introduced is less than 0.4%). In what follows, we will consider $P_3 = P_R$. Some results presented in this paper are given in term of P_3; they shall be compared to the results—also given in terms of P_3—presented in Grimal et al. (2002b). This quantity is an indicator of the energy flux propagated.

The time history of the source is, for all the computations, a Blackman window (Fig. 3) of 0.3 ms duration.

In what follows, we present: (i) displacement responses $u_1(t)$ and $u_3(t)$ in the Cartesian reference frame $(I, \mathbf{x}_1, \mathbf{x}_2, \mathbf{x}_3)$, computed in the equivalent flat representation; and (ii) $P_3(t)$ responses in the spherical representation ($\mathbf{v}_s$ and σ_s have been obtained from $\mathbf{v}_f$ and σ_f, computed in the equivalent flat representation, by using Eq. (3)).

2.5. Influence of the parameters; settings

2.5.1. Choice of the parameters

Müller (1971) has compared the displacements amplitudes calculated with the geometrical ray theory in a medium with spherical symmetry to the corresponding displacements in a flat geometry with depth dependant properties; he has shown that the FA (1) for the coordinates and velocities are optimal for the displacements amplitudes. These transformations have then been used for computations with exact and approximate theories; in this study, we have assumed that the approximation is valid for computations with the exact theory. In addition to (1), the power-law transformations defined through (2) have been used by various authors; they introduce parameters m and l. Biswas showed, by using power-laws with specific values of m and l, that the equations for Love waves—in an exact way (Biswas and Knopoff, 1970)—and for Rayleigh waves—in an approximate way (Biswas, 1972)—in flat geometry can be derived from the corresponding equations in spherical geometry. More recently, Arora et al. (1996) and Bhattacharya (1996) investigated power-laws with application to specific computational methods. Chapman (1973) attempted to find the optimum power-law parameters m and l for different wave propagation problems. It appeared that,

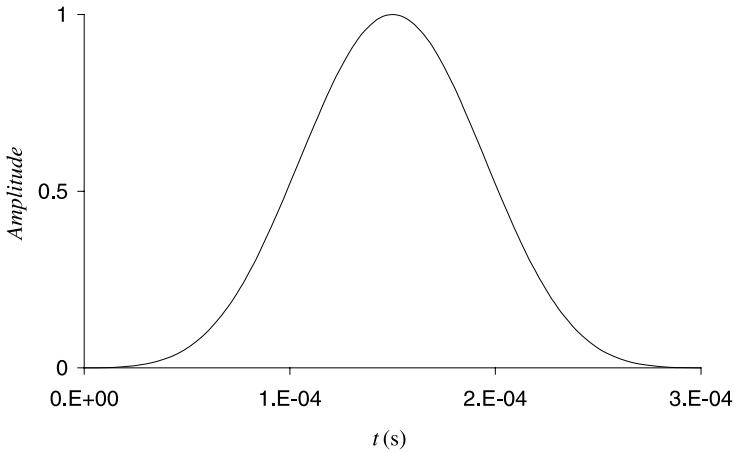

Fig. 3. Normalized time pulse shape $\phi(t)$ (Blackman window, Van der Hijden, 1987) used in the computations. The total duration of the pulse is 0.3 ms.

unlike for *SH* problems (the study of horizontally polarized shear waves) or for wave propagation in a fluid, there are no optimal values for the *P–SV* case (the coupled study of longitudinally and vertically polarized shear waves). In addition, for a given *P–SV* problem, the choice of m and l is not obvious and the estimation of the error is a difficult task. However, the FA have proved, in geophysical applications, to yield realistic results.

Before the method may be used to study a physical phenomenon, the influence of the parameters m, l and a must be investigated; this is the aim this subsection.

2.5.2. Determination of the parameter m

Chapman (1973) found, after some algebraic manipulations of the basic equations (equation of motion and constitutive law) in spherical and Cartesian coordinates, that m and l must be linked by

$$l = \frac{1-m}{2}, \tag{22}$$

hence we will only investigate the influence of m. The discussion of the parameters used in the present study is related to a biomechanical application and it probably depends on the mechanical parameters used (that is, on the length and time scales). However, the method for the determination of the parameters may be used for other cases.

Many different values of m have been used by various authors, e.g., $m = 3$ (Biswas, 1972) for an exact FA for Love waves, $m = 0$ (Biswas, 1972) for an approximate FA for Rayleigh waves, $m = -3$ (Helmberger, 1973) and $m = -2$ (Bhattacharya, 1996) for an approximate FA for body waves.

Taking $\phi(t) = H(t)$ in (21), where $H(t)$ is the Heaviside step function, the displacement in the medium is given by $(u_1, u_2, u_3) = (b_1, b_2, b_3)$, and no convolution is required. From a physical point of view, the displacement response to a step of force should show a transient phase before the static response displacement value is attained. Some responses to such a step of force in the bimaterial (whose properties are collected in Table 1) for a receiver located at $d = 0.01$ m and $z = 0.025$ m (see Fig. 1) are presented in Fig. 4a and b. They correspond to a spherical interface of radius $R_i = 0.018$ m; the source is located at point I. The responses are given for three different values of the parameter m; these figures also show for comparison the response obtained for the plane interface investigated in Grimal et al. (2002b) for the equivalent receiver ($r = 0.01$ m and $x_3 = 0.025$ m in the configuration and with the notations used in our aforementioned paper), source and interface locations. The responses are computed close to the interface, hence the effect of focalization is expected to be small, and the amplitudes corresponding to the plane and spherical interface cases should be comparable: this can be checked on the figures. The arrival times for the three plots corresponding to the spherical interface are smaller than those for the plane interface case; this is a consequence of the differences in the location of the receiver with respect to the interface. (The jagged shape of the plots for large times is due to numerical errors; those are enhanced in the computation with the FA but they have also been observed with the program dedicated to the plane interface.) The results illustrated in Fig. 4a and b enforced our choice of a value of m: the plots for $m = -3$ and $m = 3$ diverge from the plane case plot (bold line) and the corresponding responses $u_1(t)$ and $u_3(t)$ are not physically acceptable; in contrast, taking $m = 0$ seems to be a reasonable choice. However, the optimum value of m may depend on the mechanical parameters of the model.

The value of the reference radius a is chosen so that the amplitudes computed close to the spherical interface are the same as those computed close to the plane interface. The justification for this procedure is that the focalization increases with the distance from the interface; close enough to the interface, the effect of focalization should not be seen, hence the numerical calculations for the flat and spherical interfaces must give the same amplitudes. We found that the reference radius a must be equal to the distance between the source and the center of curvature O of the spherical surface.

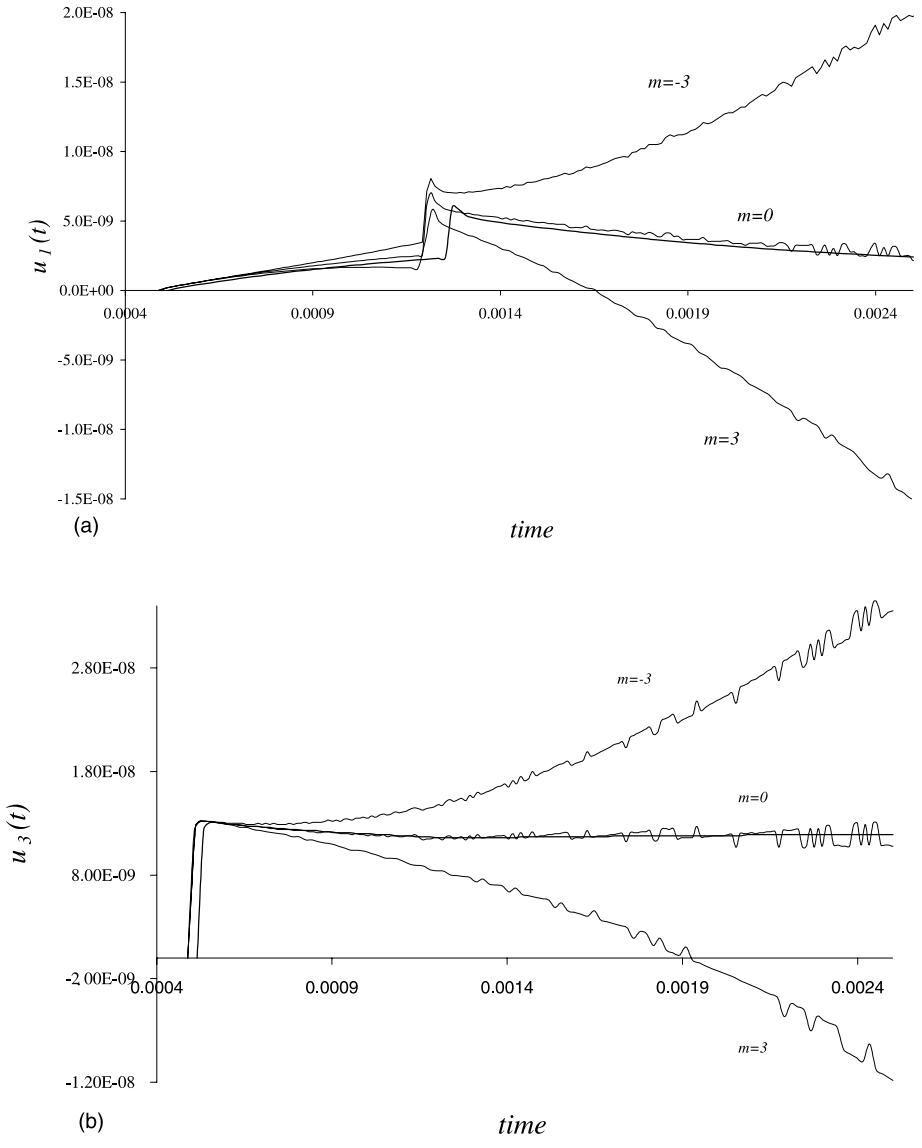

Fig. 4. Displacement responses versus time to a step of force in the spherical representation (thin line) for the receiver location $d = 0.01$ m and $z = 0.025$ m; the interface is at $R_i = 0.18$ m; the mechanical parameters are those collected in Table 1. The response obtained in the same model with a plane interface (see Grimal et al., 2002b), for a receiver location $r = 0.01$ m and $x_3 = 0.025$ m in the configuration and with the notations used in our previous paper, is represented for comparison in bold line. Among the different values considered for the parameter m, only $m = 0$ gives a physically acceptable result. (a) $u_1(t)$ and (b) $u_3(t)$. Time is in seconds.

The number of homogeneous sub-layers to introduce in the flat representation to account for the x_3-dependence of the mechanical properties is determined by testing several spatial discretizations. Fig. 5 shows the evolution of $u_3(t)$ with the number of sub-layers, for $\phi(t) = H(t)$, for a receiver located at $d = 0.005$ m and $z = 0.06$ m and for $m = 0$. It can be seen on the plots that—for the length scales of the problem under study—, it is useless to take layers thiner than 0.5 mm (the mean relative error is less than 5%).

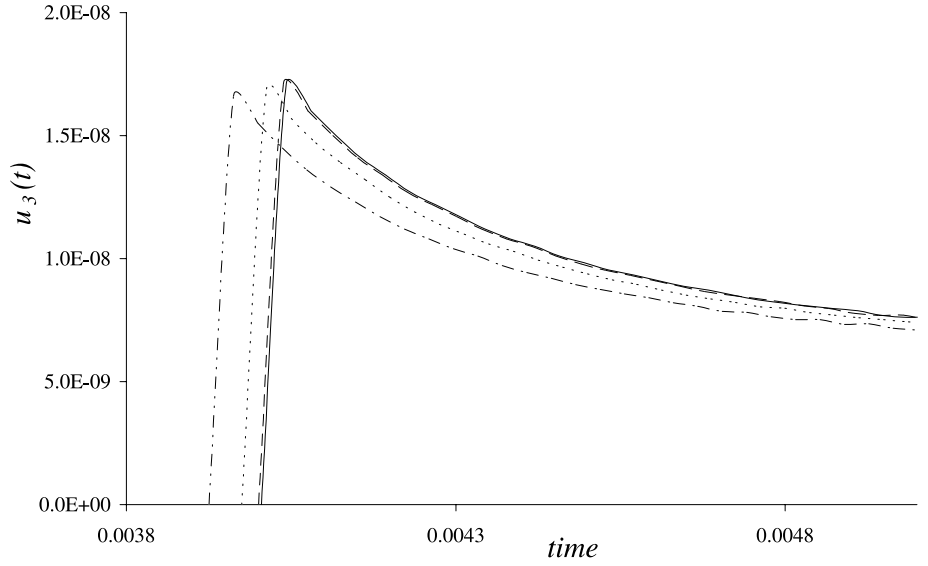

Fig. 5. Displacement responses $u_3(t)$ to a step of force, in the spherical representation for the receiver location $d = 0.005$ m and $z = 0.06$ m; the interface is at $R_i = 0.18$ m. The four plots each correspond to a spatial discretization (a given sub-layer thickness), from left to right the computation were made with: $h = 0.01$ m, $h = 0.005$ m, $h = 0.0005$ m and $h = 0.0002$ m, where h is the thickness of sub-layer. Time is in seconds.

2.6. Numerical validation

The computations whose results are illustrated in Fig. 4a and b, have proved that the method and its numerical implementation can yield physically acceptable results (for $m = 0$). Other tests have been performed to validate the method in a few simple cases.

(i) The two layers in the spherical geometry have been given the same mechanical properties so that the receiver and the buried point force are placed in a homogeneous medium. The displacement responses for a buried point force, with $\phi(t) = H(t)$, have been computed and compared with the results obtained for the model with a plane interface investigated in Grimal et al. (2002b). Displacements $u_1(t)$ and $u_3(t)$ are shown in Fig. 6a–d for $m = 0$. Since the two media have the same properties, there is no wave conversion or reflection at the interface and the transmission coefficients are equal to one. A small error is introduced in the computation of the displacement responses $u_1(t)$, at a receiver in a homogeneous medium with properties of medium 1 (Fig. 6a) or medium 2 (Fig. 6b) (see Table 1): the approximation used for the spherical model leads to a small overestimation of the displacement (less than 10%). In contrast, responses $u_3(t)$ (at a receiver in a homogeneous medium with properties of medium 1 (Fig. 6c) or medium 2 (Fig. 6d)), for the plane and spherical interfaces, are almost indistinguishable. (It is to note that the global contribution of $u_1(t)$ to the response in terms of the Poynting vector, is—at the receivers of interest in the present study—less than $u_3(t)$.) With this comparison of the displacement responses, we conclude that the change of coordinate system and of mechanical properties introduced by the flattening approximation does not perturbate the wave propagation pattern.

(ii) The computed travel times for receivers on axis $\mathbf{d}_3$ have shown good agreement with those calculated with known analytical expressions; for a sub-layer thickness of 0.5 mm, the error is less than 0.1%.

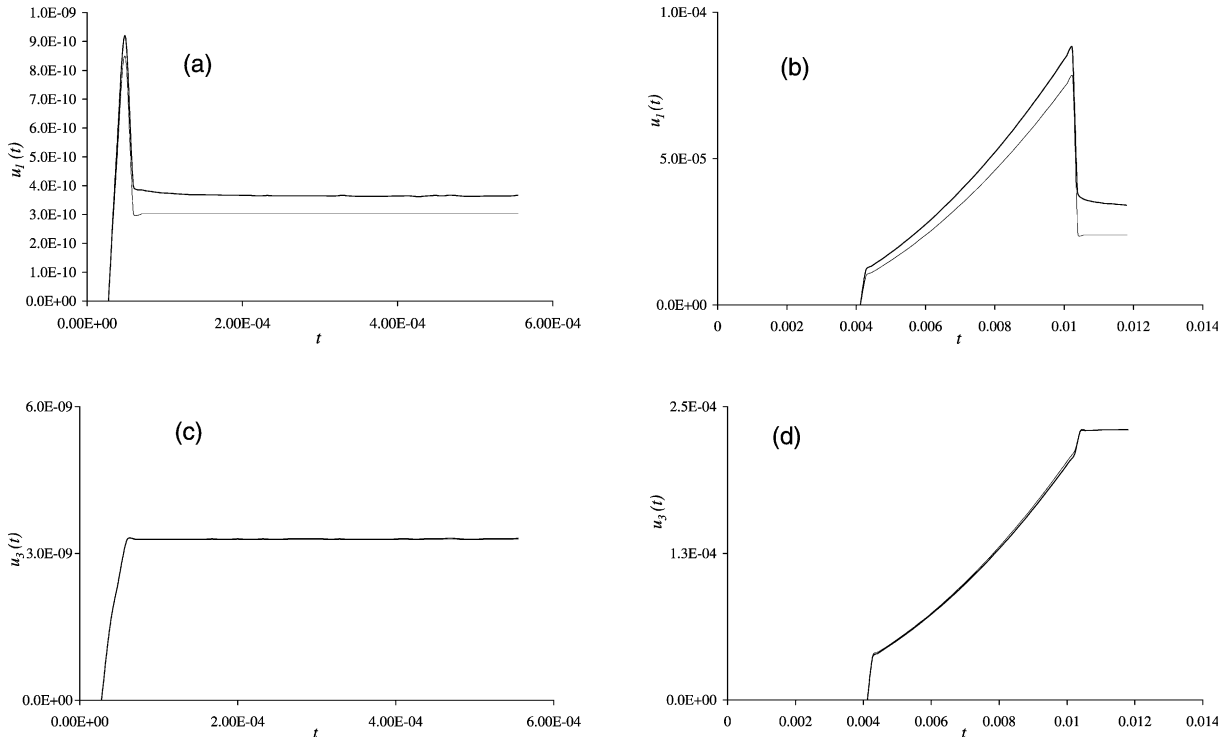

Fig. 6. Displacement responses versus time to a step of force in the spherical representation are plotted for $m = 0$ in thin line, when the receiver location is given by $d = 0.01$ m and $z = 0.04$ m. The responses obtained in the model with a plane interface (see Grimal et al., 2002b), for an equivalent receiver location, are plotted for comparison in bold line. The mechanical parameters are the same in media 1 and 2: (a) and (c) $u_1(t)$ and $u_3(t)$ by using the properties of medium 1 given in Table 1; (b) and (d) $u_1(t)$ and $u_3(t)$ by using the properties of medium 2 given in Table 1. Time is in seconds.

(iii) All the calculations of interest in this paper are concerned with a wave traveling in the direction of decreasing radius: in this case, we expect to observe focalization of energy (this is the case, as shown in the Section 3). Likewise, we have checked that waves propagating in the direction of increasing radius, decrease in amplitude with the distance from the interface, more rapidly in a model with a spherical interface than in a model with a plane interface.
(iv) Letting the radius of curvature become very large, the results found with the method including the FA converge towards the results obtained in the model with the plane interface.

The results of the aforementioned tests of the method, allow us to suppose—although there is no complete mathematical validation for this—that the set of FA can yield physically meaningful results.

3. Numerical example: repartition of energy in a model of the thorax

The impact wave generated by a "high" velocity non-penetrating impact on the thoracic wall (like when a projectile is stopped by a bulletproof jacket) is supposed to induce severe lung injuries. The detailed study of the propagation of an impact wave in the thorax is a complicated matter; the present work, which is an extension of our work presented in Grimal et al. (2002b), is part of a preliminary study whose objectives are to describe the wave propagation in a model of the thorax and to identify some phenomena involved in the mechanisms of lung injury. The specific motivation for the work presented here is to evaluate the influence

of the curvature of the thorax on the repartition of energy. In the model, the impact wave is generated by a point force at the free—spherical—surface of medium 1, the direction of the force is perpendicular to the surface (in the equivalent flat representation, the force is defined by (6)). (The way this point force accounts for the real loading of the thoracic wall will be investigated in another study.) As before, the force source is applied, normal to the free surface at 2 cm from the interface; the time history of the source is a Blackman window (Fig. 3) of 0.3 ms duration. In all the computations, we have used $m = 0$.

As for the plane interface case investigated in Grimal et al. (2002b), the wave fronts of the pressure and shear waves are found to be almost plane in medium 2; obviously, this is due to the weak acoustic coupling between media 1 and 2.

Fig. 7 shows typical plots of $P_3(t)$ for three receivers placed in medium 2 on axis $\mathbf{d}_3$; the radius of curvature of the interface is $R_i = 28$ cm (these plots may be compared to those obtained with the plane interface in Grimal et al. (2002b)). Again, the distortion of the input pulse with the distance from the source—due to the coupling of far and near-field terms—is manifest. It is to note that for receivers located near axis $\mathbf{d}_3$, the contribution of the shear waves is negligible with respect to the pressure waves contributions. The increase in amplitude with the distance from the spherical interface demonstrates the focalization of energy (this amplitude decreases with a plane interface).

Fig. 8 illustrates the influence of the radius of curvature of the interface on the degree of focalization. It shows the evolution of the maxima of the $P_3(t)$ (read on plots like Fig. 7) versus the distance from the source, at receivers in medium 2, for various interface's curvatures and for the buried explosion source used in Grimal et al. (2002b) (using a force source instead of an explosion source has little influence on the focalization pattern on axis $\mathbf{d}_3$). From the biomechanical application point of view, it is interesting to note, as displayed in Fig. 8, that P_3 weakly decreases with z for $R_i < 30$ cm. So, the focalization is pronounced for radius of curvatures of less than 30 cm, which is a value characteristic of the thoracic geometry.

In Grimal et al. (2002b), we had represented the repartition of the P- and S-waves transient strain energy contributions, denoted by $E_{P,S}$, in medium 2; the strain energy was calculated by using the formula

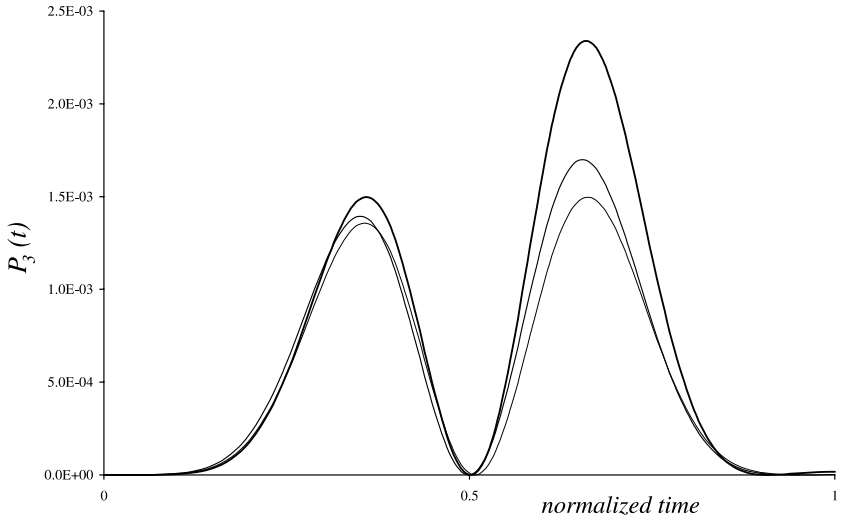

Fig. 7. $P_3(t)$ responses to a point force with the source time history illustrated in Fig. 3, for three receivers on axis $\mathbf{d}_3$; the radius of curvature of the interface is $R_i = 0.28$ m; the three values of z are: 0.025 m (thin line), 0.04 m (intermediate line) and 0.1 m (bold line). The time scale is normalized with respect to the duration of the pulse and the plots are offset of the arrival time. The amplitude of $P_3(t)$ increases with the distance from the source; this is a focalization effect due to the interface's curvature.

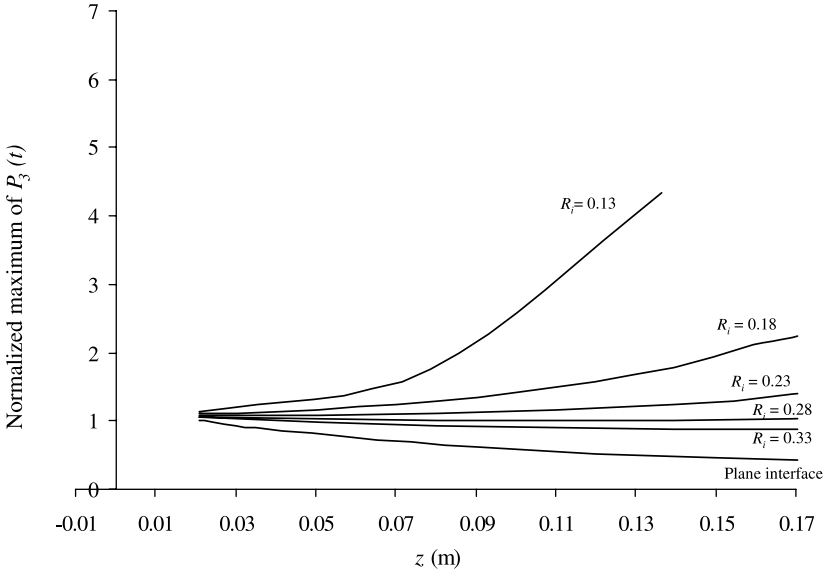

Fig. 8. Normalized maximum of $P_3(t)$ for receivers on axis $\mathbf{d}_3$ for various interface curvatures. Distances are in meters.

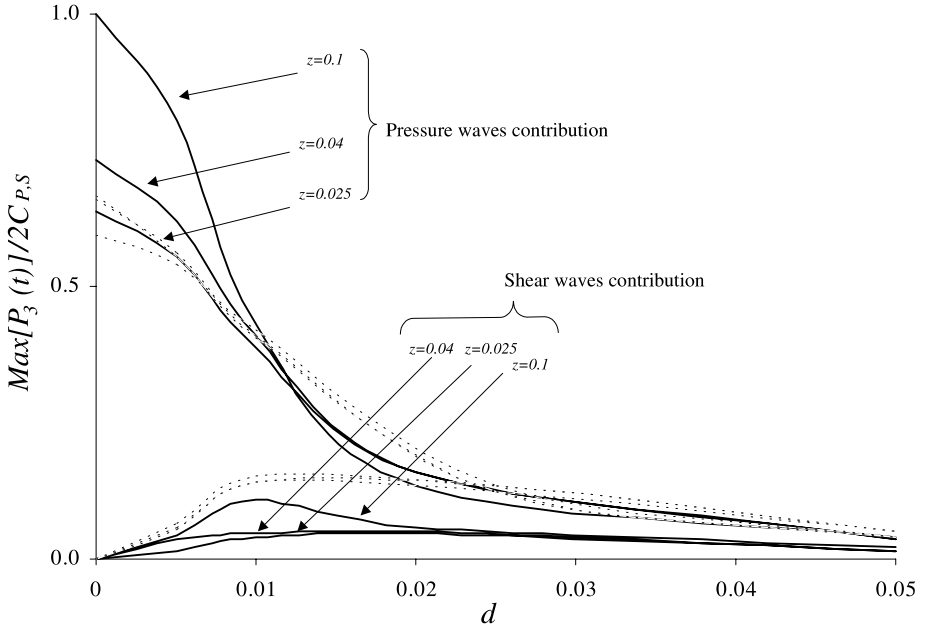

Fig. 9. Maximum of strain energy contributions (a quantity derived from $P_3(t)$) in medium 2 of P-waves (rays PP and SP) and S-waves (rays PS and SS). The source is a force at the free surface of medium 1. Continuous lines correspond to the spherical interface case ($R_i = 0.28$ m) and dotted lines to the plane interface case (Grimal et al., 2002b). Distances are in meters.

$E_{P,S} = \mathrm{Max}\,[P_3^{P,S}(t)](2c_{P,S})^{-1}$, where $\mathrm{Max}[P_3^{P,S}(t)]$ is extracted from plots like those shown in Fig. 7 (P- and S-waves contributions are well separated in time so that $P_3(t)$ can be split, without ambiguity, in two parts: $P_3^P(t)$ and $P_3^S(t)$). Fig. 9 shows the maximum transient strain energies in medium 2 for a model with a

spherical interface. Results shown in Fig. 9 correspond to a plane interface, and to an interface's curvatures of $R_i = 28$ cm; for each case, three plots corresponding to three distances z from the source are represented; the values in abscissa correspond to distances d (see Fig. 1) from the source (the choice of the coordinates (d, z) in the spherical geometry allow for comparison with the values computed for the plane interface case). In the plane interface case, the amplitudes of P- and S-waves contributions weakly decrease with the distance from the source; in contrast, in the spherical interface case, the amplitudes increase with the distance from the interface. Close to the interface ($z = 0.025$ m), there are little differences in the amplitudes of the P-waves contributions, for the plane and spherical interfaces, this illustrates that the focalization is negligible close to the interface. S-waves contributions amplitudes are smaller for the spherical case; this is probably due to differences in the receivers' locations with respect to the interface. For a point source at the free spherical surface, the focalization is shown to be important mostly close to axis $\mathbf{d}_3$, for $d > 2$ cm the plots corresponding to the two cases get superimposed.

4. Conclusion

Three-dimensional transient elastic wave propagation in a spherically symmetric bimaterial medium has been investigated. The method of solution makes use of a set of flattening transformations to build a "flat" representation equivalent—with an approximation—to the spherically symmetric representation; wave propagation is then computed with the exact three-dimensional GR/CdH method in the flat representation. Chapman (1973) has shown that FA for the coupled P–SV problems are not exact and his work proved that it is delicate to evaluate the validity of the approximation. Hence, the solution obtained in this study is only an approximation to the exact solution. However, we have checked that the results are physically acceptable and are coherent with results obtained for a bimaterial with a plane interface in a former work (Grimal et al., 2002b). Except for the work of Chapman (1973), we could not find any work discussing specifications for the choice of the parameters (m and l) of the power-law transformations given by Eq. (2). We have found optimal values by comparing the displacement responses to a step of force, for a spherical interface and a plane interface—for which the exact solution could be computed.

Flattening transformations have been widely used in geophysics to study surface waves (Love and Rayleigh waves), spheroidal modes of vibration, transient propagation of SH or P–SV body waves with many different analytical methods; however, the application of the FA to other fields of mechanical engineering is not known to the authors. We have used the FA to investigate the wave propagation in a simplified model of the thorax subjected to an impact wave loading. We have been interested in responses at receivers close to axis $\mathbf{d}_3$ in a weakly coupled bimaterial; these are the two main differences with the cases investigated by geophysicians: they rather compute responses at large horizontal distances from the source with asymptotic approximations (that are not valid in the case investigated here), and in layered media that are not weakly coupled. From the application's point of view, the results presented in this paper yield qualitative informations on the propagation of an impact wave in the thorax; in particular the results indicate that the curvature of the thoracic wall-lung interface may contribute to focalize energy: the substitution of a spherical interface of radius $R_i = 28$ cm, to a plane one, increases the energy transmitted, in the medium representing the lung, of about 50% at some points. This may play a role in the occurrence of injuries in certain curved regions of the lung.

Acknowledgement

The authors would like to thank the 'Délégation Générale pour l'Armement' of the Minister of Defense of France for supporting this work.

References

Aki, K., Richard, P.G., 1980. Quantitative Seismology: Theory and Methods. Freeman, San Francisco.

Arora, S., Bhattacharya, S.N., Gogna, M.L., 1996. Rayleigh wave dispersion equation for a layered spherical earth with exponential function solutions in each shell. Pure and Applied Geophysics 147 (3), 515–536.

Bhattacharya, S.N., 1996. Earth-flattening transformation for *P–SV* waves. Bulletin of the Seismological Society of America 86 (6), 1979–1982.

Biswas, N.N., 1972. Earth flattening procedure for the propagation of Rayleigh wave. Pure and Applied Geophysics 96, 61–74.

Biswas, N.N., Knopoff, L., 1970. Exact earth flattening calculation for Love waves. Bulletin of the Seismological Society of America 60, 1123–1137.

Chapman, C.H., 1973. Earth flattening transformation in the body wave theory. Geophysical Journal of the Royal Astronomical Society 35, 55–70.

Fung, Y.C., Yen, R.T., Tao, Z.L., Liu, S.Q., 1988. A hypothesis on the mechanism of trauma of lung tissue subjected to impact load. Journal of Biomechanical Engineering 110, 50–56.

Gilbert, F., Helmberger, D.B., 1972. Generalized rat theory for a layered sphere. Geophysical Journal of the Royal Astronomical Society 27, 57–80.

Grimal, Q., Naili, S., Watzky, A., 2002a. A study of impact wave propagation in the thorax. Mechanics Research Communications 29, 73–80.

Grimal, Q., Naili, S., Watzky, A., 2002b. A study of transient elastic wave propagation in a bimaterial modeling the thorax. International Journal of Solid and Structures 39, 5345–5369.

Helmberger, D.V., 1973. Numerical seismograms of long period body waves from seventeen to forty degrees. Bulletin of the Seismological Society of America 63, 633–645.

Kennett, B.L.N., 1983. Seismic Wave Propagation in Stratified Media. Cambridge University Press.

Müller, G., 1971. Approximate treatment of elastic body waves in media with spherical symmetry. Geophysical Journal of the Royal Astronomical Society 23, 435–449.

Pao, Y., Gajewski, R., 1977. The generalized ray theory and transient response of layered elastic solids. In: Mason, W.P. (Ed.), Physical Acoustics, vol. 13, pp. 184–265.

Van der Hijden, J.H.M.T., 1987. Propagation of transient elastic waves in stratified anisotropic media. North Holland Series in Applied Mathematics and Mechanics, vol. 32.

Yen, R.T., Fung, Y.C., Liu, S.Q., 1988. Trauma of the lung due to impact load. Journal of Biomechanics 21, 745–753.